INTERNATIONAL JOURNAL FOR NUMERICAL METHODS IN FLUIDS, VOL. 9, 75–98 (1989)

FINITE DIFFERENCE METHODS FOR SOLVING THE TWO-DIMENSIONAL ADVECTION–DIFFUSION EQUATION

B. J. NOYE AND H. H. TAN

Department of Applied Mathematics, Adelaide University, North Terrace, Adelaide, South Australia 5000, Australia

SUMMARY

Using weighted discretization with the modified equivalent partial differential equation approach, several accurate finite difference methods are developed to solve the two-dimensional advection–diffusion equation following the success of its application to the one-dimensional case. These new methods are compared with the conventional finite difference methods in terms of stability and accuracy. The new methods are more accurate and often more stable than the conventional schemes.

KEY WORDS 2D Advection–diffusion equation Finite difference method Weighted discretization Modified equivalent PDE approach Stability Accuracy

1. INTRODUCTION

In this article the two-dimensional advection–diffusion equation

$$\frac{\partial \hat{t}}{\partial t} + u\frac{\partial \hat{t}}{\partial x} + v\frac{\partial \hat{t}}{\partial y} - \alpha_x \frac{\partial^2 \hat{t}}{\partial x^2} - \alpha_y \frac{\partial^2 \hat{t}}{\partial y^2} = 0 \tag{1}$$

is considered in the domain $0 \le x \le \theta$, $0 \le y \le \xi$ with θ and ξ fixed, where $\hat{t}(x, y, t)$ is a transported (advected and diffused) scalar variable, $u > 0$ and $v > 0$ being constant speeds of advection and $\alpha_x > 0$ and $\alpha_y > 0$ being constant diffusivities in the x- and y-direction respectively. Various numerical techniques such as the finite difference and finite element methods have been used in the past to solve (1) approximately. Finite difference methods (FDMs), including both conventional and some new ones developed here, will be compared theoretically and in practice. Dirichlet boundary conditions will be imposed on (1), so the values of $\hat{t}(0, y, t)$, $\hat{t}(\theta, y, t)$, $\hat{t}(x, 0, t)$ and $\hat{t}(x, \xi, t)$ will be assumed known with the initial condition $\hat{t}(x, y, 0)$ given.

Equation (1) is a linearized version of the partial differential equations which describe advection–diffusion of quantities such as mass, heat, energy, vorticity, etc. For example, equation (1) has been used to describe heat transfer in a draining film,[1] water transfer in soils,[2] dispersion of tracers in porous media,[3] the intrusion of salt water into fresh water aquifers,[4] the spread of pollutants in rivers and streams,[5] the dispersion of dissolved material in estuaries and coastal seas,[6] contaminant dispersion in shallow lakes,[7] the spread of solute in a liquid flowing through a tube,[8] long-range transport of pollutants in the atmosphere[9] and forced cooling by fluids of solid material such as windings in turbo generators.[10]

0271–2091/89/010075–24$12.00

Received 8 May 1987
Revised 8 March 1988

The advection–diffusion equation in both one- and multi-dimensional forms has been solved using FDMs for the transient as well as the steady case.[11,12] Recently a new technique involving weighted discretization and the modified equivalent partial differential equation (MEPDE) has been successfully used to develop highly accurate finite difference equations (FDEs) for the one-dimensional advection equation,[13,14] the one-dimensional diffusion equation[15] and the one-dimensional advection–diffusion equation.[16–18] In this paper the technique is extended to produce several new FDMs for solving the two-dimensional transient advection–diffusion equation (1).

2. THE MODIFIED EQUIVALENT PARTIAL DIFFERENTIAL EQUATION

Consider the finite difference equation (FDE)

$$L_\Delta[\tau^n_{j,k}]=0 \tag{2}$$

in which L_Δ is a finite difference operator and $\tau^n_{j,k}=\tau(j\Delta x, k\Delta y, n\Delta t)$ is the numerical approximation to $\hat{\tau}(j\Delta x, k\Delta y, n\Delta t)$, $j=0(1)J$, $k=0(1)K$, $n=0(1)N$, $\Delta x=\theta/J$, $\Delta y=\xi/K$, $\Delta t=T/N$, where $T=N\Delta t$ is the final time at which a solution is required. If (2) is consistent with (1), then a Taylor series expansion about the (j, k, n)th gridpoint for each term in (2) will give an equivalent partial differential equation (EPDE) of the form

$$\frac{\partial\tau}{\partial t}+u\frac{\partial\tau}{\partial x}+v\frac{\partial\tau}{\partial y}-\alpha_x\frac{\partial^2\tau}{\partial x^2}-\alpha_y\frac{\partial^2\tau}{\partial y^2}+\sum_{p=2}^{\infty}\sum_{q=0}^{p}\sum_{r=0}^{q}F_{r,q-r,p-q}\frac{\partial^p\tau}{\partial t^r\partial x^{q-r}\partial y^{p-q}}=0, \tag{3}$$

which is the partial differential equation actually solved by (2). The summed terms in (3) form the truncation error which indicates the order of accuracy of the FDE (2). Similar to the one-dimensional case, the MEPDE is obtained from the EPDE by converting all derivatives of (3) involving $\partial/\partial t$, except $\partial\tau/\partial t$, into derivatives of x and y only. The truncation error of the MEPDE then includes only derivatives in x or y or both. There are therefore fewer terms of the same order to be dealt with in the MEPDE than in the EPDE. The procedure of obtaining the MEPDE from the EPDE for the one-dimensional case and its PASCAL implementation are described in Noye and Hayman.[16] The extension of this procedure to the two-dimensional case has been implemented and used extensively in the work leading up to this paper.

The general form of the MEPDE for (1) is given by

$$\frac{\partial\tau}{\partial t}+u\frac{\partial\tau}{\partial x}+v\frac{\partial\tau}{\partial y}-\alpha_x\frac{\partial^2\tau}{\partial x^2}-\alpha_y\frac{\partial^2\tau}{\partial y^2}+\sum_{p=2}^{\infty}\sum_{q=0}^{p}C_{q,p-q}\frac{\partial^p\tau}{\partial x^q\partial y^{p-q}}=0, \tag{4}$$

where the terms under the summation signs form the truncation error. Note that for each p there is a total of $p+1$ derivatives of the same order involved in the MEPDE.

In the following, a FDM is said to have accuracy of rth order if $C_{p,p-q}=0$, $q=0(1)p$, for all $p=2(1)r$, where at least one $C_{r+1,r+1-q}\neq 0$, $q=0(1),r+1$. The notation $q=0(1)p$ indicates that q takes all integers from 0 to p, in steps of 1. If any of $C_{2,2-q}\neq 0$, $q=0(1)2$, then the coefficients α_x and/or α_y are altered and/or a term involving $\partial^2\tau/\partial x\partial y$ is introduced, so some form of numerical diffusion or anti-diffusion is incorporated in the method. The method is first-order accurate in this case.

Using weighted differencing in order to construct higher-order schemes,[17,18] weights are used to eliminate from the MEPDE as many as possible of the terms containing the derivatives $\partial^p\tau/\partial x^q\partial y^{p-q}$, $q=1(1)p-1$, $p=2, 3, \ldots$, to develop FDMs of higher orders of accuracy than conventional methods.

In the following, the notation (n_1, n_2) will be used to denote a stencil with n_1 gridpoints at the $(n+1)$th time level and n_2 gridpoints at the nth time level. The stencils to be used for explicit methods in this paper are the (1, 5) and (1, 9) stencils shown in Figure 1. The (5, 5) and (9, 9) stencils illustrated in Figure 2 will be used for implicit methods in this work. In addition, two semi-implicit methods will also be developed using the (2, 5) and (2, 9) stencils shown in Figure 3.

3. SOME CONVENTIONAL METHODS

The FTCS explicit method

The FTCS (forward time, centred space) FDM is based on the (1, 5) computational stencil shown in Figure 1(a). It uses centred space (CS) difference forms for all the spatial derivatives and the forward time (FT) difference form for the time derivative. The FDE so obtained is

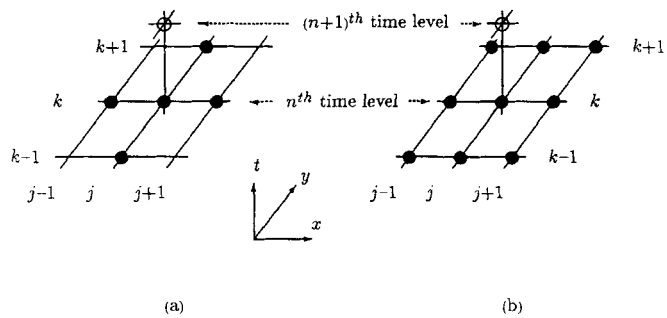

Figure 1. The (a) (1, 5) and (b) (1, 9) stencils

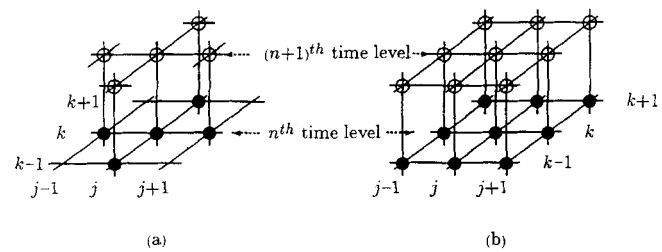

Figure 2. The (a) (5, 5) and (b) (9, 9) stencils

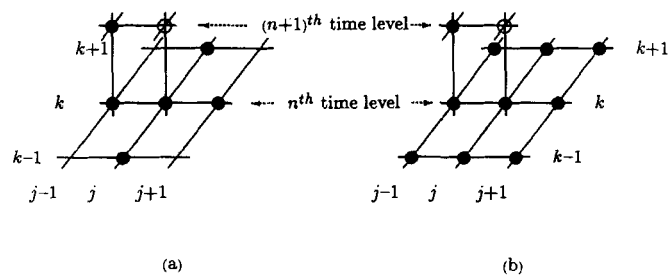

Figure 3. The (a) (2, 5) and (b) (2, 9) stencils

$$\tau_{j,k}^{n+1}=(c_x/2)(2R_{\Delta x}^{-1}+1)\tau_{j-1,k}^{n}+(c_y/2)(2R_{\Delta y}^{-1}+1)\tau_{j,k-1}^{n}+(1-2c_xR_{\Delta x}^{-1}-2c_yR_{\Delta y}^{-1})\tau_{j,k}^{n}$$
$$+(c_y/2)(2R_{\Delta y}^{-1}-1)\tau_{j,k+1}^{n}+(c_x/2)(2R_{\Delta x}^{-1}-1)\tau_{j+1,k}^{n}, \tag{5}$$

where $c_x=u\Delta t/\Delta x$, $c_y=v\Delta t/\Delta y$ are Courant-type numbers and $R_{\Delta x}=u\Delta x/\alpha_x$, $R_{\Delta y}=v\Delta y/\alpha_y$ are Reynolds numbers. The MEPDE of this FDE has the coefficients of the leading (first-order) error terms given by

$$C_{2,0}=u\Delta xc_x/2, \qquad C_{1,1}=uv\Delta t, \qquad C_{0,2}=v\Delta yc_y/2. \tag{6}$$

This implies that the FTCS method introduces numerical diffusion in both the x- and y-directions as well as that due to the cross-derivative term $\partial^2\tau/\partial x\partial y$. Clearly this method is only first-order accurate.

Application of von Neumann stability analysis[19] shows that (5) is stable if

$$c_xR_{\Delta x}^{-1}+c_yR_{\Delta y}^{-1}\leq\tfrac{1}{2} \tag{7}$$

and

$$c_xR_{\Delta x}+c_yR_{\Delta y}\leq 2. \tag{8}$$

If $R_{\Delta x}=R_{\Delta y}=R_\Delta$ and $c_x=c_y=c$, these **yield the stability condition**

$$4c\leq R_\Delta\leq c^{-1}, \tag{9}$$

which is more restrictive than the corresponding criteria for the one-dimensional FTCS FDM.[17] The stability region for (9) is shown by the vertically shaded region in Figure 4.

The upwind explicit method

The upwind method also uses the (1, 5) computational stencil, but with backward space (BS) difference forms for the spatial derivatives in the advective terms, CS difference forms for the derivatives in the diffusion terms and the FT difference form for the time derivative. The FDE so obtained is

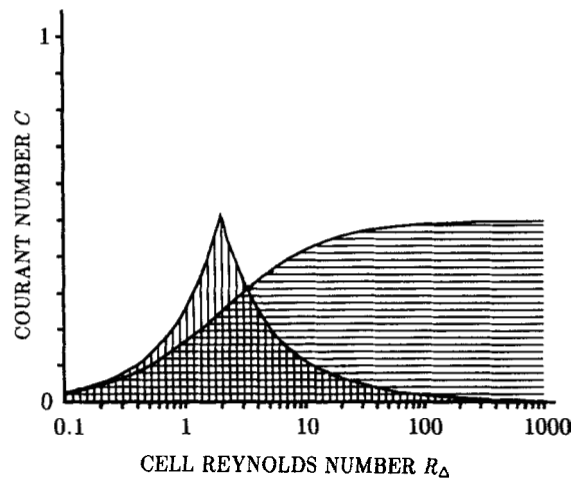

Figure 4. The von Neumann stability region in the (R_Δ, c) plane for the FTCS (vertical lines) and the upwind method (horizontal lines)

$$\tau_{j,k}^{n+1} = c_x(R_{\Delta x}^{-1}+1)\tau_{j-1,k}^{n} + c_y(R_{\Delta y}^{-1}+1)\tau_{j,k-1}^{n} + [1-c_x(1+2R_{\Delta x}^{-1})-c_y(1+2R_{\Delta y}^{-1})]\tau_{j,k}^{n} + c_x R_{\Delta x}^{-1}\tau_{j+1,k}^{n} + c_y R_{\Delta y}^{-1}\tau_{j,k+1}^{n}, \tag{10}$$

for which the leading (first-order) error terms in the MEPDE (4) have coefficients given by

$$C_{2,0} = -u\Delta x(1-c_x)/2, \qquad C_{1,1} = uv\Delta t, \qquad C_{0,2} = -v\Delta y(1-c_y)/2. \tag{11}$$

Therefore the upwind method is first-order accurate and, like the FTCS method, introduces numerical diffusion in the x- and y-directions as well as that due to the coefficient $C_{1,1}$. Application of the von Neumann stability analysis[19] shows that the stability requirement for (10) is

$$c_x(2R_{\Delta x}^{-1}+1)+c_y(2R_{\Delta y}^{-1}+1)\leq 1. \tag{12}$$

If $c_x=c_y=c$ and $R_{\Delta x}=R_{\Delta y}=R_\Delta$, this condition becomes

$$R_\Delta \geq 4c/(1-2c), \tag{13}$$

which is twice as restrictive as in the one-dimensional case discussed in Noye and Tan.[17] The stability region for (13) is shown by the horizontal shading in Figure 4.

The Crank–Nicolson-type implicit method

Discretizing (1) at the point midway between the (j, k, n)th and the $(j, k, n+1)$th gridpoints and replacing the spatial derivatives by the average of their values at the nth and the $(n+1)$th time levels, using centred difference forms for all derivatives, gives the Crank–Nicolson-type (5, 5) FDE

$$\begin{aligned} &c_y(2R_{\Delta y}^{-1}+1)\tau_{j,k-1}^{n+1} + c_x(2R_{\Delta x}^{-1}+1)\tau_{j-1,k}^{n+1} - 4(1+c_xR_{\Delta x}^{-1}+c_yR_{\Delta y}^{-1})\tau_{j,k}^{n+1} \\ &\quad + c_x(2R_{\Delta x}^{-1}-1)\tau_{j+1,k}^{n+1} + c_y(2R_{\Delta y}^{-1}-1)\tau_{j,k+1}^{n+1} \\ &= -c_y(2R_{\Delta y}^{-1}+1)\tau_{j,k-1}^{n} - c_x(2R_{\Delta x}^{-1}+1)\tau_{j-1,k}^{n} - 4(1-c_xR_{\Delta x}^{-1}-c_yR_{\Delta y}^{-1})\tau_{j,k}^{n} \\ &\quad - c_x(2R_{\Delta x}^{-1}-1)\tau_{j+1,k}^{n} - c_y(2R_{\Delta y}^{-1}-1)\tau_{j,k+1}^{n}. \end{aligned} \tag{14}$$

This FDM is second-order accurate since

$$C_{2,0}=C_{1,1}=C_{0,2}=0 \tag{15a}$$

in its MEPDE and coefficients of the second-order error terms are

$$\begin{aligned} C_{3,0} &= u(\Delta x)^2(2+c_x^2)/12, & C_{2,1} &= u^2v(\Delta t)^2/4, \\ C_{1,2} &= v^2u(\Delta t)^2/4, & C_{0,3} &= u(\Delta y)^2(2+c_y^2)/12. \end{aligned} \tag{15b}$$

A stability analysis shows that (14) is unconditionally stable. The implicit FDE may be solved by application of the Thomas[20] algorithm adapted for use on the resulting block tridiagonal system. Stability of this process is assured if the system is diagonally dominant, that is if

$$4(1+c_xR_{\Delta x}^{-1}+c_yR_{\Delta y}^{-1}) \geq c_y(2R_{\Delta y}^{-1}+1)+c_x(2R_{\Delta x}^{-1}+1)+|c_x(2R_{\Delta x}^{-1}-1)|+|c_y(2R_{\Delta y}^{-1}-1)| \tag{16}$$

(see Feingold and Varga[21]). For simplicity, assuming that $R_{\Delta x}=R_{\Delta y}=R_\Delta$ and $c_x=c_y=c$, this solvability condition becomes

$$R_\Delta \leq 2c/(c-1). \tag{17}$$

4. IMPROVED EXPLICIT (1,5) AND SECOND-ORDER (1,9) METHODS

Improved (1, 5) explicit method

For the (1, 5) stencil, two weights ϕ, γ can be meaningfully introduced through the use of the forward time approximation applied to $\partial\hat{\tau}/\partial t$ and the centred space approximation applied to $\partial^2\hat{\tau}/\partial x^2$, $\partial^2\hat{\tau}/\partial y^2$ at the (j, k, n)th gridpoint, with the following weighted forms for the advective derivatives:

$$\frac{\partial\hat{\tau}}{\partial x} \approx \phi \times \mathrm{BS} + (1-\phi) \times \mathrm{CS}, \qquad \frac{\partial\hat{\tau}}{\partial y} \approx \gamma \times \mathrm{BS} + (1-\gamma) \times \mathrm{CS}. \tag{18}$$

The weighted FDE so obtained is

$$\begin{aligned}\tau_{j,k}^{n+1} = {} & (c_x/2)(\phi + 1 + 2R_{\Delta x}^{-1})\tau_{j-1,k}^{n} + (c_x/2)(\phi - 1 + 2R_{\Delta x}^{-1})\tau_{j+1,k}^{n} \\ & + (1 - \phi c_x - \gamma c_y - 2c_x R_{\Delta x}^{-1} - 2c_y R_{\Delta y}^{-1})\tau_{j,k}^{n} \\ & + (c_y/2)(\gamma + 1 + 2R_{\Delta y}^{-1})\tau_{j,k-1}^{n} + (c_y/2)(\gamma - 1 + 2R_{\Delta y}^{-1})\tau_{j,k+1}^{n}.\end{aligned} \tag{19}$$

The leading (first-order) error terms in the MEPDE for (19) have the coefficients

$$C_{2,0} = u\Delta x(-\phi + c_x)/2, \qquad C_{1,1} = uv\Delta t, \qquad C_{0,2} = v\Delta y(-\gamma + c_y)/2. \tag{20}$$

The numerical diffusion introduced by the first and last of these may be eliminated by setting $\phi = c_x$ and $\gamma = c_y$, but there still remains a first-order error term involving $\partial^2\tau/\partial x\partial y$. The resulting improved first-order FDE for this (1, 5) stencil is

$$\begin{aligned}\tau_{j,k}^{n+1} = {} & (c_x/2)(1 + c_x + 2R_{\Delta x}^{-1})\tau_{j-1,k}^{n} + (c_x/2)(c_x - 1 + 2R_{\Delta x}^{-1})\tau_{j+1,k}^{n} \\ & + [1 - c_x(c_x + 2R_{\Delta x}^{-1}) - c_y(c_y + 2R_{\Delta y}^{-1})]\tau_{j,k}^{n} \\ & + (c_y/2)(c_y - 1 + 2R_{\Delta y}^{-1})\tau_{j,k+1}^{n} + (c_y/2)(c_y + 1 + 2R_{\Delta y}^{-1})\tau_{j,k-1}^{n},\end{aligned} \tag{21}$$

which is the two-dimensional version of the Lax–Wendroff[22] method.

A von Neumann stability analysis[19] indicates that (21) is stable for values of $R_{\Delta x}$, $R_{\Delta y}$, c_x, c_y which satisfy

$$R_{\Delta x} R_{\Delta y} c_x c_y \leq 4 \tag{22a}$$

and

$$c_x(R_{\Delta x}^{-1} + c_x) + c_y(R_{\Delta y}^{-1} + c_y) \leq 1. \tag{22b}$$

For $R_{\Delta x} = R_{\Delta y} = R_\Delta$ and $c_x = c_y = c$, these become

$$4c/(1 - 2c^2) \leq R_\Delta \leq 2/c, \tag{23}$$

which is the region of the (R_Δ, c) plane shown by the horizontal shading in Figure 5. This stability region is larger than that for the FTCS method, but is smaller than that of the upwind method, particularly for large R_Δ.

A second-order (1, 9) explicit method

To obtain FDMs of greater accuracy, more gridpoints must be used in order to introduce extra weights so that more terms in the truncation error of the MEPDE (4) may be eliminated. Adding four extra gridpoints $(j-1, k-1, n)$, $(j-1, k+1, n)$, $(j+1, k-1, n)$ and $(j+1, k+1, n)$ to the (1, 5) stencil of Figure 1(a), it becomes the (1, 9) stencil of Figure 1(b) and the error terms involving $\partial^2\tau/\partial x\partial y$ in the MEPDE of (21) may be eliminated by using the approximation

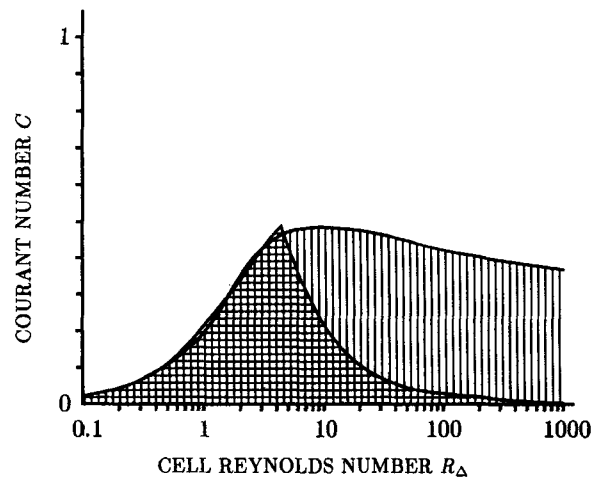

Figure 5. The von Neumann stability region in the (R_Δ, c) plane for the explicit (1, 9) method (vertical lines) and the explicit (1, 5) method (horizontal lines)

$$\left.\frac{\partial^2\tau}{\partial x\partial y}\right|_{j,k}^{n} \approx \frac{1}{4\Delta x\Delta y}(-\tau_{j-1,k+1}^{n}+\tau_{j+1,k+1}^{n}+\tau_{j-1,k-1}^{n}-\tau_{j+1,k-1}^{n}), \tag{24}$$

which has a truncation error of $O\{(\Delta x)^2, (\Delta y)^2\}$. The method of obtaining a more accurate FDE through replacement of error terms in the MEPDE has been described for the one-dimensional case by Noye and Hayman.[16] Consider the finite difference equation (21) written in the form

$$L_\Delta[\tau_{j,k}^{n}]=0, \tag{25a}$$

where

$$L_\Delta[\tau_{j,k}^{n}]\equiv\tau_{j,k}^{n+1}-a_{-1,0}\tau_{j-1,k}^{n}-a_{1,0}\tau_{j+1,k}^{n}-a_{0,0}\tau_{j,k}^{n}-a_{0,1}\tau_{j,k+1}^{n}-a_{0,1}\tau_{j,k-1}^{n} \tag{25b}$$

in which $a_{-1,0}$, $a_{1,0}$, $a_{0,0}$, $a_{0,1}$ and $a_{0,-1}$ are the corresponding coefficients in (21). Using the results in (20) with $\phi=c_x$ and $\gamma=c_y$, this may be written in the alternative differential form

$$L_\Delta[\tau_{j,k}^{n}]\equiv\Delta t\left(\frac{\partial\tau}{\partial t}+u\frac{\partial\tau}{\partial x}+v\frac{\partial\tau}{\partial y}-\alpha_x\frac{\partial^2\tau}{\partial x^2}-\alpha_y\frac{\partial^2\tau}{\partial y^2}+uv\Delta t\frac{\partial^2\tau}{\partial x\partial y}+\ldots\right)\Bigg|_{j,k}^{n}. \tag{25c}$$

Subtracting the error term $uv(\Delta t)^2\partial^2\tau/\partial x\partial y$ from (25c) is equivalent to subtracting from (25b) the term

$$c_xc_y(-\tau_{j-1,k+1}^{n}+\tau_{j+1,k+1}^{n}+\tau_{j-1,k-1}^{n}-\tau_{j+1,k-1}^{n})/4. \tag{26}$$

The largest error terms in the brackets on the right-hand side of (25c) are now $O\{(\Delta x)^2, (\Delta y)^2\}$. Rearrangement gives the second-order (1, 9) FDE

$$\tau_{j,k}^{n+1}=\sum_{p=-1}^{1}\sum_{q=-1}^{1}a_{p,q}\tau_{j+p,k+q}^{n} \tag{27a}$$

in which

$$\begin{aligned}&a_{-1,-1}(c_x, c_y)=-a_{-1,1}(c_x, c_y)=-a_{1,-1}(c_x, c_y)=a_{1,1}(c_x, c_y)=c_xc_y/4,\\ &a_{-1,0}(c_x, R_{\Delta x})=a_{0,-1}(c_y, R_{\Delta y})=-a_{0,1}(-c_y, -R_{\Delta y})=a_{1,0}(-c_x, -R_{\Delta x})=c_x(1+c_x+2R_{\Delta x}^{-1})/2.\end{aligned} \tag{27b}$$

The MEPDE of equation (27) contains no first-order error terms and has the following coefficients of the second-order error terms:

$$\begin{aligned} C_{3,0} &= u(\Delta x)^2[1-c_x(c_x+6R_{\Delta x}^{-1})]/6, \\ C_{2,1} &= -v(\Delta x)^2 c_x(1+2R_{\Delta x}^{-1})/2, \\ C_{1,2} &= -u(\Delta y)^2 c_y(1+2R_{\Delta y}^{-1})/2, \\ C_{0,3} &= v(\Delta y)^2[1-c_y(c_y+6R_{\Delta y}^{-1})]/6. \end{aligned} \tag{28}$$

Setting $R_{\Delta x}=R_{\Delta y}=R_\Delta$, $c_x=c_y=c$ and carrying out a numerical stability analysis yields the stability region in the (R_Δ, c) plane shown by the vertical shading in Figure 5. This is a larger stability region than either the FTCS (1, 5) or the Lax–Wendroff method. It is comparable in size to the first-order upwind method.

5. ALTERNATIVE SECOND-ORDER (5,5) METHODS AND A THIRD-ORDER (9,9) METHOD

Using the (5, 5) stencil of Figure 2(a) with CS difference forms for all spatial derivatives in (1) and the following approximation to the time derivative involving two weights η and ε,

$$\begin{aligned} \frac{\partial \hat{\tau}}{\partial t} \approx \eta &\left[\frac{\tau_{j,k+1}^{n+1}-\tau_{j,k+1}^{n}}{\Delta t}+\frac{\tau_{j,k-1}^{n+1}-\tau_{j,k-1}^{n}}{\Delta t}\right]+\varepsilon\left[\frac{\tau_{j-1,k}^{n+1}-\tau_{j-1,k}^{n}}{\Delta t}+\frac{\tau_{j+1,k}^{n+1}-\tau_{j+1,k}^{n}}{\Delta t}\right] \\ &+(1-2\varepsilon-2\eta)\left[\frac{\tau_{j,k}^{n+1}-\tau_{j,k}^{n}}{\Delta t}\right], \end{aligned} \tag{29}$$

gives the FDE

$$\sum_{p=-1}^{1}\sum_{q=-1}^{1} a_{p,q}\tau_{j+p,k+q}^{n+1} = \sum_{p=-1}^{1}\sum_{q=-1}^{1} b_{p,q}\tau_{j+p,k+q}^{n+1}, \tag{30a}$$

with $a_{p,q}=b_{p,q}=0$ if $p\neq 0$ and $q\neq 0$ and

$$\begin{aligned} &a_{-1,0}(c_x, R_{\Delta x}) = b_{-1,0}(-c_x, R_{\Delta x}) = \varepsilon - c_x/4(1+2R_{\Delta x}^{-1}), \\ &a_{0,-1}(c_y, R_{\Delta y}) = b_{0,-1}(-c_y, R_{\Delta y}) = \eta - c_y/4(1+2R_{\Delta y}^{-1}), \\ &a_{0,0}(c_x, c_y, R_{\Delta x}, R_{\Delta y}) = (1-2\eta-2\varepsilon+c_xR_{\Delta x}^{-1}+c_yR_{\Delta y}^{-1}), \\ &b_{0,0}(c_x, c_y, R_{\Delta x}, R_{\Delta y}) = a_{0,0}(-c_x, -c_y, R_{\Delta x}, R_{\Delta y}), \\ &a_{0,1}(c_y, R_{\Delta y}) = b_{0,1}(-c_y, R_{\Delta y}) = \eta + c_y/4(1-2R_{\Delta y}^{-1}), \\ &a_{1,0}(c_x, R_{\Delta x}) = b_{1,0}(-c_x, R_{\Delta x}) = \varepsilon + c_x/4(1-2R_{\Delta x}^{-1}). \end{aligned} \tag{30b}$$

The MEPDE of this FDE has leading error terms with coefficients given by

$$\begin{aligned} &C_{2,0}=C_{1,1}=C_{0,2}=0, \\ &C_{3,0}=u(\Delta x)^2(12\varepsilon-2-c_x^2)/12, \qquad C_{2,1}=v(\Delta x)^2(4\varepsilon-c_x^2)/4, \\ &C_{1,2}=u(\Delta y)^2(4\eta-c_y^2)/4, \qquad C_{0,3}=v(\Delta y)^2(12\eta-2-c_y^2)/12, \end{aligned} \tag{31}$$

which means that no numerical diffusion is introduced by the method. However, only two of the four second-order terms can be eliminated with the two weights available. Four different FDMs can be obtained by setting any two of the four terms equal to zero.

For example, setting $C_{2,1}=C_{1,2}=0$ gives $\varepsilon=c_x^2/4$, $\eta=c_y^2/4$ with

$$C_{3,0}=u(\Delta x)^2(1-c_x^2)/6, \qquad C_{0,3}=v(\Delta y)^2(1-c_y^2)/6. \tag{32}$$

The resultant second-order FDE has the form (30a) with

$$\begin{aligned} a_{-1,0}(c_x, R_{\Delta x}) &= a_{0,-1}(c_y, R_{\Delta y}) = a_{1,0}(-c_x, -R_{\Delta x}) = a_{0,1}(-c_y, -R_{\Delta y}) \\ &= c_x(c_x - 1 - 2R_{\Delta x}^{-1}), \\ a_{0,0}(c_x, c_y, R_{\Delta x}, R_{\Delta y}) &= 2[2 - c_x(c_x - 2R_{\Delta x}^{-1}) - c_y(c_y - 2R_{\Delta y}^{-1})]. \end{aligned} \tag{33}$$

A numerically implemented von Neumann stability analysis with $R_{\Delta x} = R_{\Delta y} = R_\Delta$ and $c_x = c_y = c$ gives the stability region in the (R_Δ, c) plane indicated by the vertical shading in Figure 6. This method is stable for all R_Δ and $c \leq 0{\cdot}8$. Diagonal dominance of (33) with $R_{\Delta x} = R_{\Delta y} = R_\Delta$ and $c_x = c_y = c$ gives the solvability region in the (R_Δ, c) plane shown by the horizontal shading in Figure 6. The usable region is therefore the cross-hatched area in this figure.

Setting $C_{3,0} = C_{0,3} = 0$ gives

$$\varepsilon = (2 + c_x^2)/12, \qquad \eta = (2 + c_y^2)/12, \tag{34}$$

but the resulting second-order FDE is always unstable in the von Neumann sense so it will not be considered further.

Setting $C_{3,0} = C_{1,2} = 0$ gives

$$\varepsilon = (2 + c_x^2)/12, \qquad \eta = c_y^2/4, \tag{35}$$

so that

$$C_{2,1} = v(\Delta x)^2(c_x^2 - 1)/6, \qquad C_{0,3} = v(\Delta y)^2(1 - c_y^2)/6 \tag{36}$$

and the resulting second-order FDE has the form (30a) with

$$\begin{aligned} a_{-1,0}(c_x, R_{\Delta x}) &= a_{1,0}(-c_x, -R_{\Delta x}) = 2 + c_x(c_x - 3 - 6R_{\Delta x}^{-1}), \\ a_{0,-1}(c_y, R_{\Delta y}) &= a_{0,1}(-c_y, -R_{\Delta y}) = 3c_y(c_y - 1 - 2R_{\Delta y}^{-1}), \\ a_{0,0}(c_x, c_y, R_{\Delta x}, R_{\Delta y}) &= 2[4 - 3c_y(c_y - 2R_{\Delta y}^{-1}) - c_x(c_x - 6R_{\Delta x}^{-1})]. \end{aligned} \tag{37}$$

A numerical stability analysis of (37) in the simplified case considered for the previous FDMs yields the vertically shaded stability region in the (R_Δ, c) plane shown in Figure 7; that is, (37) is

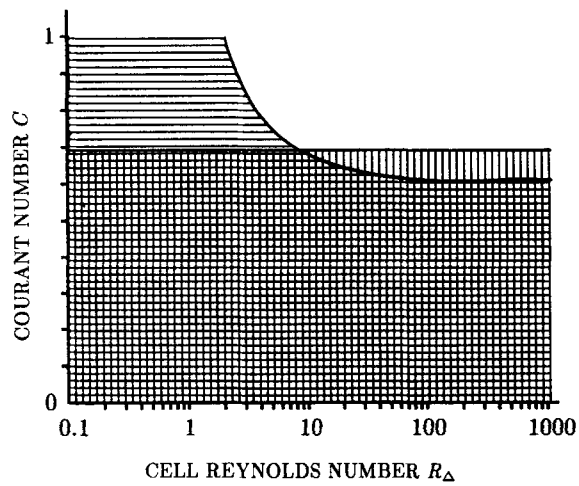

Figure 6. The regions of von Neumann stability (vertical lines) and diagonal dominance (horizontal lines) for the alternative (5, 5) method, equation (33)

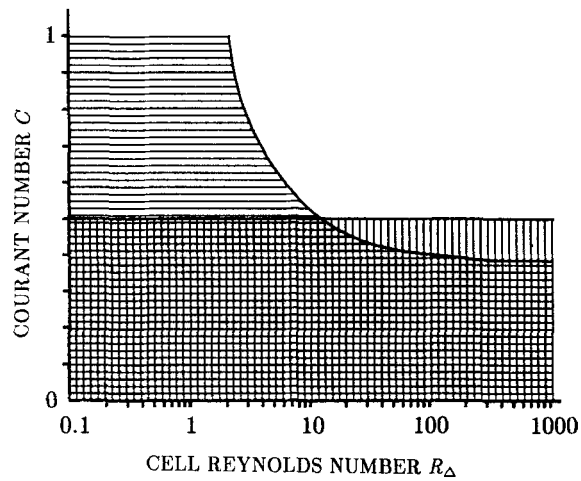

Figure 7. The regions of von Neumann stability (vertical lines) and diagonal dominance (horizontal lines) for the alternative (5, 5) method, equation (37)

stable for $c \leq 0{\cdot}5$ and all R_Δ, which is a smaller region than that of FDE (33). The solvability region of (37) in the (R_Δ, c) plane is indicated by the horizontal shading in Figure 7. The cross-hatched region gives the values of (R_Δ, c) which may be used in practice.

Setting $C_{0,3} = C_{2,1} = 0$ gives

$$\varepsilon = c_x^2/4, \qquad \eta = (2 + c_y^2)/12, \tag{38}$$

so that

$$C_{1,2} = u(\Delta y)^2(c_y^2 - 1)/6, \qquad C_{3,0} = v(\Delta x)^2(1 - c_x^2)/6. \tag{39}$$

The resulting second-order FDE has the form shown in (30a) with

$$\begin{aligned} a_{-1,0}(c_x, R_{\Delta x}) &= a_{1,0}(-c_x, R_{\Delta x}) = 3c_x(c_x - 1 - 2R_{\Delta x}^{-1}), \\ a_{0,-1}(c_y, R_{\Delta y}) &= a_{0,1}(-c_y, -R_{\Delta y}) = 2 + c_y(c_y - 3 - 6R_{\Delta y}^{-1}), \\ a_{0,0}(c_x, c_y, R_{\Delta x}, R_{\Delta y}) &= 2[4 - c_y(c_y - 6R_{\Delta y}^{-1}) - 3c_x(c_x - 2R_{\Delta x}^{-1})]. \end{aligned} \tag{40}$$

A numerical stability analysis of (40) yields the same stability region in the (R_Δ, c) plane as for FDE (37) in Figure 7. The solvability region of (40) is also the same as for (37).

A third-order (9, 9) implicit method

In the following, the (9, 9) stencil in Figure 2(b) is used to develop a third-order (9, 9) FDM for solving (1). Eight weights, namely β, δ, ε, μ, ϕ, η, γ and χ, are used to cope with the many possible difference forms which may be used with 18 gridpoints. Discretizing (1) at the midpoint between the (j, k, n)th gridpoint and the $(j, k, n+1)$th gridpoint means that centred time (CT) difference forms of second order may be used for approximating $\partial\hat{t}/\partial t$. Four weights are used in the nine possible centred time approximations to $\partial\hat{t}/\partial t$ in a manner similar to that used in equation (29), that is

$$\left.\frac{\partial \hat{t}}{\partial t}\right|_{j,k}^{n+1/2} \approx \delta \times [\text{CT at } (j-1, k+1)] + \eta \times [\text{CT at } (j, k+1)] + \beta \times [\text{CT at } (j+1, k+1)] + \varepsilon \times [\text{CT at } (j-1, k)] + (1-2\eta-2\varepsilon-2\delta-2\beta) \times [\text{CT at } (j, k)]. + \varepsilon \times [\text{CT at } (j+1, k)] + \beta \times [\text{CT at } (j-1, k-1)] + \eta \times [\text{CT at } (j, k-1)] + \delta \times [\text{CT at } (j+1, k-1)]. \tag{41}$$

The average of the spatial derivatives at the two time levels n and $n+1$ is taken and four weights ϕ, μ, γ and χ are used in the discretization of each derivative in the following manner:

$$\left.\frac{\partial \hat{t}}{\partial x}\right|_{j,k}^{n+1/2} \approx [\phi \times \text{CS at } (k-1, n) + (1-2\phi) \times \text{CS at } (k, n) + \phi \times \text{CS at } (k+1, n)]/2 + [\phi \times \text{CS at } (k-1, n+1) + (1-2\phi) \times \text{CS at } (k, n+1) + \phi \times \text{CS at } (k+1, n+1)]/2, \tag{42a}$$

$$\left.\frac{\partial \hat{t}}{\partial y}\right|_{j,k}^{n+1/2} \approx [\mu \times \text{CS at } (j-1, n) + (1-2\mu) \times \text{CS at } (j, n) + \mu \times \text{CS at } (j+1, n)]/2 + [\mu \times \text{CS at } (j-1, n+1) + (1-2\mu) \times \text{CS at } (j, n+1) + \mu \times \text{CS at } (j+1, n+1)]/2, \tag{42b}$$

$$\left.\frac{\partial^2 \hat{t}}{\partial x^2}\right|_{j,k}^{n+1/2} \approx [\gamma \times \text{CS at } (k-1, n) + (1-2\gamma) \times \text{CS at } (k, n) + \gamma \times \text{CS at } (k+1, n)]/2 + [\gamma \times \text{CS at } (k-1, n+1) + (1-2\gamma) \times \text{CS at } (k, n+1) + \gamma \times \text{CS at } (k+1, n+1)]/2, \tag{43a}$$

$$\left.\frac{\partial^2 \hat{t}}{\partial y^2}\right|_{j,k}^{n+1/2} \approx [\chi \times \text{CS at } (j-1, n) + (1-2\chi) \times \text{CS at } (j, n) + \chi \times \text{CS at } (j+1, n)]/2 + [\chi \times \text{CS at } (j-1, n+1) + (1-2\chi) \times \text{CS at } (j, n+1) + \chi \times \text{CS at } (j+1, n+1)]/2. \tag{43b}$$

In this way, a (9,9) FDE containing the eight weights is found, the MEPDE of which has leading error terms with zero values for $C_{2,0}$, $C_{1,1}$ and $C_{0,2}$ and

$$\begin{aligned} C_{3,0} &= [u(\Delta x)^2/6][1-6(\delta+\beta+\varepsilon)+c_x^2/2], \\ C_{2,1} &= v(\Delta x)^2(\mu-\delta-\beta-\varepsilon)+(u\Delta x\Delta y/4)[8(\delta-\beta)+c_x c_y], \\ C_{1,2} &= u(\Delta y)^2(\phi-\delta-\eta-\beta)+(v\Delta x\Delta y/4)[8(\delta-\beta)+c_x c_y], \\ C_{0,3} &= [v(\Delta y)^2/6][1-6(\delta+\eta+\beta)+c_y^2/2], \end{aligned} \tag{44a}$$

with

$$\begin{aligned} C_{4,0} &= u(\Delta x)^3[-1+12(\delta+\beta+\varepsilon)-3c_x^2]/(12R_{\Delta x}), \\ C_{3,1} &= -u(\Delta x)^2\Delta y[4(\delta-\beta)+c_x c_y]/(2R_{\Delta x}), \\ C_{2,2} &= u\Delta x(\Delta y)^2[4(\beta+\eta+\delta-\gamma)-c_y^2]/(4R_{\Delta x})+v\Delta y(\Delta x)^2[4(\beta+\varepsilon+\delta-\chi)-c_x^2]/(4R_{\Delta y}), \\ C_{1,3} &= -v\Delta x(\Delta y)^2[4(\delta-\beta)+c_x c_y]/(2R_{\Delta y}), \\ C_{0,4} &= v(\Delta y)^3[-1+12(\delta+\eta+\beta)-3c_y^2]/(12R_{\Delta y}). \end{aligned} \tag{44b}$$

Note that the second-order derivatives have no error terms in them, a fact due to the spatially symmetrical CT weighting scheme for $\partial\hat{t}/\partial t$. It is also noteworthy that solving $C_{3,1}=0$ and $C_{1,3}=0$ are equivalent.

It is obvious that $C_{3,0}$ and $C_{4,0}$ cannot both be zero at the same time, nor can $C_{0,3}$ and $C_{0,4}$. This leaves six non-linear equations involving eight weights. Choosing the weights

$$\begin{aligned}
&\delta=(2+c_x^2-12\varepsilon-3c_xc_y)/24, && \beta=(2+c_x^2-12\varepsilon+3c_xc_y)/24,\\
&\eta=(c_y^2-c_x^2)/12+\varepsilon, && \mu=(2c_x^2+1)/6, \qquad \phi=(2c_y^2+1)/6,\\
&\gamma=(1-c_y^2)/6, && \chi=(1-c_x^2)/6,
\end{aligned} \tag{45}$$

gives $C_{3,0}=C_{2,1}=C_{1,2}=C_{0,3}=C_{3,1}=C_{1,3}=C_{2,2}=0$. Substituting the weights in (47) into the weighted (9,9) FDE gives a third-order accurate (9,9) FDE containing the weight ε, namely

$$\begin{aligned}
&(A-12\varepsilon+D+E-Q)\tau_{j-1,k-1}^{n+1}-4(V-6\varepsilon-P)\tau_{j-1,k}^{n+1}\\
&\quad+(A-12\varepsilon-D+E-Q)\tau_{j-1,k+1}^{n+1}-2(B-H+I-12\varepsilon)\tau_{j,k-1}^{n+1}\\
&\quad+4(B+L+M-12\varepsilon)\tau_{j,k}^{n+1}-2(B+H+I-12\varepsilon)\tau_{j,k+1}^{n+1}\\
&\quad+(A-W+G+Q-12\varepsilon)\tau_{j+1,k-1}^{n+1}-4(V+P-6\varepsilon)\tau_{j+1,k}^{n+1}\\
&\quad+(A+W+G+Q-12\varepsilon)\tau_{j+1,k+1}^{n+1}+(A+12\varepsilon-W-G-Q)\tau_{j-1,k-1}^{n}\\
&\quad-4(V-P+6\varepsilon)\tau_{j-1,k}^{n}+(A+W-G-Q+12\varepsilon)\tau_{j-1,k+1}^{n}\\
&\quad-2(B-H-I+12\varepsilon)\tau_{j,k-1}^{n}+4(B+L-M+12\varepsilon)\tau_{j,k}^{n}\\
&\quad-2(B+H-I+12\varepsilon)\tau_{j,k+1}^{n}+(A+D-E+Q+12\varepsilon)\tau_{j+1,k-1}^{n}\\
&\quad-4(V+P+6\varepsilon)\tau_{j+1,k}^{n}+(A-D-E+Q+12\varepsilon)\tau_{j+1,k+1}^{n}=0,
\end{aligned} \tag{46a}$$

in which

$$\begin{aligned}
&A=2c_yR_{\Delta y}^{-1}(c_x^2-1)+2c_xR_{\Delta x}^{-1}(c_y^2-1), && B=2c_yR_{\Delta y}^{-1}(c_x^2+2)+2c_xR_{\Delta x}^{-1}(c_y^2-1),\\
&V=c_yR_{\Delta y}^{-1}(c_x^2-1)+c_xR_{\Delta x}^{-1}(c_y^2+2), && D=-2c_x^2c_y+3c_xc_y-c_y,\\
&E=c_x^2-c_x+2, && W=2c_x^2c_y+3c_xc_y+c_y, \qquad G=c_x^2+c_x+2,\\
&H=2c_x^2c_y-2c_y, && I=-c_y^2+c_x^2, \qquad P=c_xc_y^2-c_x,\\
&Q=2c_xc_y^2, && L=6c_xR_{\Delta x}^{-1}, \qquad M=-c_y^2+4.
\end{aligned} \tag{46b}$$

The MEPDE of the FDE (46) has the coefficients of all third-order derivatives equal to zero and those of the fourth-order derivatives are

$$\begin{aligned}
&C_{4,0}=u(\Delta x)^3(1-2c_x^2)/(12R_{\Delta x}),\\
&C_{3,1}=C_{2,2}=C_{1,3}=0,\\
&C_{0,4}=v(\Delta y)^3(1-2c_y^2)/(12R_{\Delta y}),
\end{aligned} \tag{47}$$

which are independent of ε; hence one can set ε to zero for simplicity in (46) without altering the leading error terms. The (9,9) FDE (46) can be solved using the block Thomas algorithm referred to earlier.

Although ε plays an insignificant role in the order of accuracy of the FDE, it can be used to determine the best stability region. Assuming $R_{\Delta x}=R_{\Delta y}=R_\Delta$ and $c_x=c_y=c$, stability regions in the (R_Δ,c) plane for $\varepsilon=0$ and 0·1 have been found. They are shown in Figures 8 and 9 by means of vertical shading. The requirement of diagonal dominance of (46) in the same simplified case gives the solvability regions in the (R_Δ, c) plane for $\varepsilon=0$ and 0·1 shown by the horizontal shading in Figures 8 and 9.

After testing various values of ε, it was found that $\varepsilon=0$ gave the best combined solvability region and stability region among the values of ε tested, so the value $\varepsilon=0$ was used in (46) for the numerical tests described in Section 7.

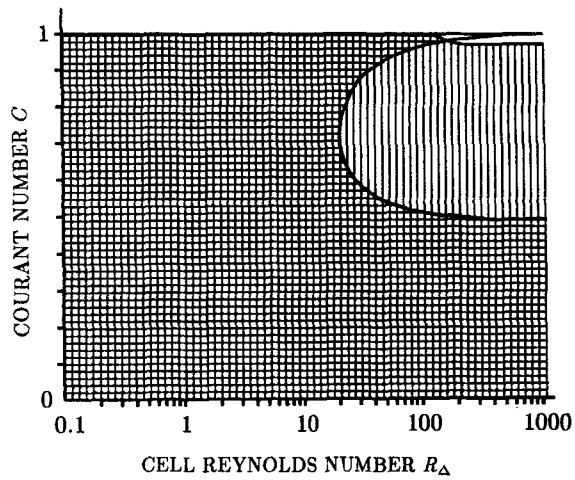

Figure 8. The regions of von Neumann stability (vertical lines) and diagonal dominance (horizontal lines) for the third-order (9, 9) method for $\varepsilon = 0$

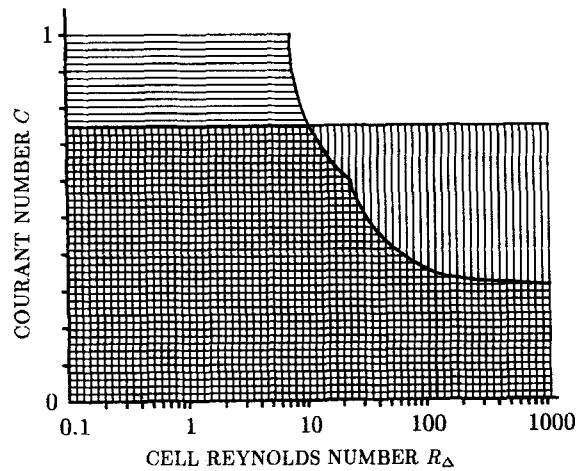

Figure 9. The regions of von Neumann stability (vertical lines) and diagonal dominance (horizontal lines) for the third-order (9, 9) method for $\varepsilon = 0{\cdot}1$

6. SEMI-IMPLICIT METHODS

If in an implicit method there are only two unknowns in a given co-ordinate direction at the new time level in the stencil used, then the FDE based upon it can be solved efficiently in an explicit manner by marching across the grid in that direction at the new time level. This combines the advantage of increased time-stepping stability of implicit methods with the advantage of the speed of computation of explicit FDMs. In this section, the (2, 5) and (2, 9) stencils shown in Figure 3 are used to develop two such semi-implicit FDMs.

A second-order (2,5) semi-implicit method

Consider firstly (1) discretized on the (2, 5) stencil using three weights γ, ϕ and β in the following manner:

$$\begin{aligned}
&\left.\frac{\partial \hat{t}}{\partial t}\right|_{j,k}^{n} \approx \gamma \times [\text{FT at } (j-1,k)] + (1-\gamma) \times [\text{FT at } (j,k)],\\
&\left.\frac{\partial \hat{t}}{\partial x}\right|_{j,k}^{n} \approx \phi \times [\text{BS using } (j-1,k) \text{ and } (j,k)] + (1-\phi) \times [\text{CS from } (j-1,k) \text{ to } (j+1,k)],\\
&\left.\frac{\partial \hat{t}}{\partial y}\right|_{j,k}^{n} \approx \beta \times [\text{BS using } (j,k-1) \text{ and } (j,k)] + (1-\beta) \times [\text{CS from } (j,k-1) \text{ to } (j,k+1)],\\
&\left.\frac{\partial^2 \hat{t}}{\partial x^2}\right|_{j,k}^{n} \approx \text{CS from } (j-1,k) \text{ to } (j+1,k),\\
&\left.\frac{\partial^2 \hat{t}}{\partial y^2}\right|_{j,k}^{n} \approx \text{CS from } (j,k-1) \text{ to } (j,k+1).
\end{aligned} \tag{48}$$

Using these approximations yields a weighted FDE which has the MEPDE with coefficients of the errors involving the second-order derivatives given by

$$\begin{aligned}
C_{2,0} &= u\Delta x(-\phi + 2\gamma - \phi c_x + c_x)/2,\\
C_{1,1} &= v\Delta x(2c_x + 2\gamma - \phi c_x)/2,\\
C_{0,2} &= v\Delta y(\beta + c_y)/2.
\end{aligned} \tag{49}$$

Setting $C_{2,0} = C_{1,1} = C_{0,2} = 0$ yields the following values for the weights:

$$\phi = -c_x, \qquad \beta = -c_y, \qquad \gamma = -c_x(c_x+2)/2. \tag{50}$$

Substitution of these in the weighted FDE gives the second-order (2, 5) FDE

$$\begin{aligned}
-2c_x\tau^{n+1}_{j-1,k} + 2(1+c_x)\tau^{n+1}_{j,k} = {} & c_x(2R^{-1}_{\Delta x} - c_x - 1)\tau^{n}_{j-1,k} + c_y(2R^{-1}_{\Delta y} + c_y + 1)\tau^{n}_{j,k-1}\\
& + 2[1 - c_x(2R^{-1}_{\Delta x} - c_x - 1) - c_y(2R^{-1}_{\Delta y} + c_y)]\tau^{n}_{j,k}\\
& + c_y(2R^{-1}_{\Delta y} + c_y - 1)\tau^{n}_{j,k+1} + c_x(2R^{-1}_{\Delta x} - c_x - 1)\tau^{n}_{j+1,k}.
\end{aligned} \tag{51}$$

This equation has the MEPDE for which the coefficients of the leading (second-order) error terms are given by

$$\begin{aligned}
C_{3,0} &= u(\Delta x)^2(1 + 2c_x^2 + 3c_x)/6,\\
C_{2,1} &= v(\Delta x)^2 c_x(-2R^{-1}_{\Delta x} + c_x + 1)/2,\\
C_{1,2} &= 0,\\
C_{0,3} &= v(\Delta y)^2[1 - c_y(c_y + 6R^{-1}_{\Delta y})]/6.
\end{aligned} \tag{52}$$

Given known boundary values $\tau^{n+1}_{0,k}$, equation (51) can be used to march across the grid in the x-direction for each value of $k = 1(1)K-1$. Investigating the stability of this marching procedure requires $|1+c_x| > |1-c_x|$, which is always true as $c_x > 0$. Thus (51) is always marchable.

A numerical stability analysis of (51) in the simplified case $c_x = c_y = c$, $R_{\Delta x} = R_{\Delta y} = R_\Delta$ considered earlier yields the stability region in the (R_Δ, c) plane shown in Figure 10. This region is very restricted especially for large values of cell Reynolds numbers.

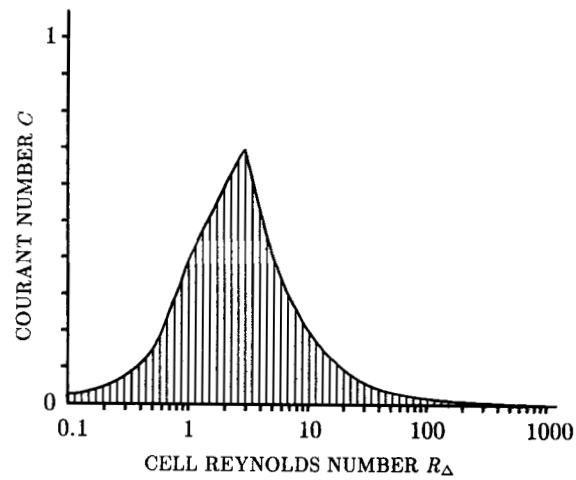

Figure 10. The von Neumann stability region of the (2, 5) second-order semi-implicit method

An alternative discretization on the (2, 9) stencil using seven weights $\beta, \phi, \varepsilon, \delta, \omega, \mu$ and γ may be achieved in the following manner:

$$\left.\frac{\partial \hat{t}}{\partial t}\right|_{j,k}^{n} \approx \beta \times [\text{FT at } (j-1,\ k)] + (1-\beta) \times [\text{FT at } (j,\ k)],$$

$$\begin{aligned}\left.\frac{\partial \hat{t}}{\partial x}\right|_{j,k}^{n} \approx\ & \{\varepsilon \times [\text{BS using } (j-1,\ k+1) \text{ and } (j,\ k+1)] \\ & + (\phi-\varepsilon) \times [\text{CS using } (j-1,\ k+1) \text{ and } (j+1,\ k+1)]\} \\ & + \{\delta \times [\text{BS using } (j-1,\ k) \text{ and } (j+1,\ k)] \\ & + (1-2\phi-\delta) \times [\text{CS using } (j-1,\ k) \text{ to } (j+1,\ k)]\} \\ & + \{\varepsilon \times [\text{BS using } (j-1,\ k-1) \text{ and } (j,\ k-1)] \\ & + (\phi-\varepsilon) \times [\text{CS using } (j-1,\ k-1) \text{ and } (j+1,\ k-1)]\},\end{aligned} \tag{53}$$

$$\begin{aligned}\left.\frac{\partial \hat{t}}{\partial y}\right|_{j,k}^{n} \approx\ & \{\omega \times [\text{BS using } (j-1,\ k-1) \text{ and } (j-1,\ k)] \\ & + (\gamma-\omega) \times [\text{CS using } (j-1,\ k-1) \text{ and } (j-1,\ k+1)]\} \\ & + \{\mu \times [\text{BS using } (j,\ k-1) \text{ and } (j,\ k)] \\ & + (1-\mu-2\gamma) \times [\text{CS using } (j,\ k-1) \text{ to } (j,\ k+1)]\} \\ & + \{\omega \times [\text{BS using } (j+1,\ k-1) \text{ and } (j+1,\ k)] \\ & + (\gamma-\omega) \times [\text{CS using } (j+1,\ k-1) \text{ and } (j+1,\ k+1)]\},\end{aligned}$$

$$\left.\frac{\partial^2 \hat{t}}{\partial x^2}\right|_{j,k}^{n} \approx \phi \times (\text{CS at } k+1) + (1-2\phi) \times (\text{CS at } k) + \phi \times (\text{CS at } k-1),$$

$$\left.\frac{\partial^2 \hat{t}}{\partial y^2}\right|_{j,k}^{n} \approx \gamma \times (\text{CS at } j+1) + (1-2\gamma) \times (\text{CS at } j) + \gamma \times (\text{CS at } j-1).$$

Substituting these approximations into equation (1) yields a weighted (2, 9) FDE which has the MEPDE with coefficients of the leading error terms given by

$$\begin{aligned} C_{1,1} &= v\Delta x(c_x+\beta),\\ C_{2,0} &= u\Delta x(-2\varepsilon+2\beta-\delta+c_x)/2,\\ C_{0,2} &= v\Delta y(-2\omega-\mu+c_y)/2 \end{aligned} \tag{54}$$

and

$$\begin{aligned} C_{3,0} &= u(\Delta x)^2(1+3c_x+2c_x^2)/6\neq 0,\\ C_{2,1} &= v(\Delta x)^2(2\gamma-2\varepsilon c_x-\delta c_x-2c_xR_{\Delta x}^{-1}+c_x)/2,\\ C_{1,2} &= u(\Delta y)^2\phi,\\ C_{0,3} &= v(\Delta y)^2(1-6\omega c_y-3\mu c_y-6c_yR_{\Delta y}^{-1}+2c_y^2)/6. \end{aligned} \tag{55}$$

Note that $C_{3,0}$ is never zero since $\Delta x\neq 0$ and only one of $C_{2,0}$ and $C_{0,3}$ can be made zero. Setting $C_{2,0}=C_{1,1}=C_{0,2}=C_{2,1}=C_{1,2}=0$ yields the weights

$$\begin{aligned} &\phi=0, \qquad \beta=-c_x, \qquad \varepsilon=-(\delta+c_x)/2,\\ &\omega=(c_y-\mu)/2, \qquad \gamma=c_x[R_{\Delta x}^{-1}-(\delta+c_x+1)/2]. \end{aligned} \tag{56}$$

There appears to be two free weights in this system, but on substitution back into the weighted (2, 9) FDE, a second-order (2, 9) FDE is obtained which contains no weights, namely

$$-2c_x\tau_{j-1,k}^{n+1}+2(1+c_x)\tau_{j,k}^{n+1}=\sum_{p=-1}^{1}\sum_{q=-1}^{1}a_{p,q}\tau_{j+p,k+q}^{n} \tag{57a}$$

in which

$$\begin{aligned} &a_{-1,-1}(c_x, c_y, R_{\Delta x})=a_{-1,1}(c_x, -c_y, R_{\Delta x})=-(c_x^2-c_y^2-2c_xc_yR_{\Delta x}^{-1}+c_x^2c_y+c_xc_y)/2,\\ &a_{-1,0}(c_x, c_y, R_{\Delta x})=-(c_x+c_y^2-2c_xR_{\Delta x}^{-1}),\\ &a_{0,-1}(c_x, c_y, R_{\Delta x}, R_{\Delta y})=(c_x^2-2c_xc_yR_{\Delta x}^{-1}+c_x^2c_y+c_xc_y+c_y+2c_yR_{\Delta y}^{-1}),\\ &a_{0,0}(c_x, c_y, R_{\Delta x}, R_{\Delta y})=-2(2c_xR_{\Delta x}^{-1}+2c_yR_{\Delta y}^{-1}-1-c_x),\\ &a_{0,1}(c_x, c_y, R_{\Delta x}, R_{\Delta y})=-a_{0,-1}(c_x, -c_y, R_{\Delta x}, -R_{\Delta y}),\\ &a_{1,-1}=a_{-1,-1}, \qquad a_{1,0}=a_{-1,0}, \qquad a_{1,1}=a_{-1,1}. \end{aligned} \tag{57b}$$

The coefficients of the second-order error terms in the MEPDE of (57a) are given by

$$\begin{aligned} C_{3,0} &= u(\Delta x)^2(1+2c_x^2+3c_x)/6,\\ C_{2,1} &= C_{1,2}=0,\\ C_{0,3} &= v(\Delta y)^2[1-c_y(c_y+R_{\Delta y}^{-1})]/6. \end{aligned} \tag{58}$$

The coefficients of $\tau_{j-1,k}^{n+1}$ and $\tau_{j,k}^{n+1}$ in (57) are the same as in (51) and therefore (57) is also always marchable. Also, a numerical stability analysis of (57) gives the same stability region in the (R_Δ, c) plane as for (51) illustrated in Figure 10.

The second-order errors in both the (2, 5) and (2, 9) methods may be reduced by marching in the positive x-direction using (51) and (57) and then in the negative x-direction using (51) and (57), with $-\Delta x$ replacing Δx at alternative time levels. For example, (51) becomes

$$\begin{aligned} 2(1-c_x)\tau_{j,k}^{n+1}+2c_x\tau_{j+1,k}^{n+1}= &-c_x(2R_{\Delta x}^{-1}+c_x+1)\tau_{j-1,k}^{n}+c_y(2R_{\Delta y}^{-1}+c_y-1)\tau_{j,k-1}^{n}\\ &+2[1+c_x(2R_{\Delta x}^{-1}+c_x+1)-c_y(2R_{\Delta y}^{-1}+c_y)]\tau_{j,k}^{n}\\ &+c_y(2R_{\Delta y}^{-1}-c_y-1)\tau_{j,k+1}^{n}-c_x(2R_{\Delta x}^{-1}+c_x+1)\tau_{j+1,k}^{n} \end{aligned} \tag{59}$$

for the march in the negative x-direction.

7. A NUMERICAL TEST CASE

To test FDMs developed for solving (1), a special problem for which an analytic solution is available must be obtained. In detail, (1) is solved in the rectangular region $x \in [0, 2]$ and $y \in [0, 2]$ with the initial condition

$$\hat{\tau}(x, y, 0) = \exp\left(- \frac{(x-0{\cdot}5)^2}{\alpha_x} - \frac{(y-0{\cdot}5)^2}{\alpha_y} \right). \tag{60}$$

An analytic solution to the above problem is

$$\hat{\tau}(x, y, t) = \frac{1}{4t+1} \exp\left(- \frac{(x-ut-0{\cdot}5)^2}{\alpha_x(4t+1)} - \frac{(y-vt-0{\cdot}5)^2}{\alpha_y(4t+1)} \right). \tag{61}$$

Since Dirichlet boundary conditions are assumed for this rectangular region, the appropriate boundary values of $\tau(x, y, t)$ are obtained directly from (61).

The initial condition (60) is a two-dimensional Gauss pulse centred at $(x, y) = (0{\cdot}5, 0{\cdot}5)$ with a pulse height of 1. Choosing $\alpha_x = \alpha_y = 0{\cdot}01$ and $u = v = 0{\cdot}8$, then at $t = 1{\cdot}25$ this pulse will have moved to a position centred at $(x, y) = (1{\cdot}5, 1{\cdot}5)$ with a pulse height of $\frac{1}{6}$. The initial condition and the pulse at $t = 1{\cdot}25$ are illustrated in Figure 11; the initial condition is shown in the region $(x, y) \in (0, 1) \times (0, 1)$ and the exact solution in the region $(x, y) \in (1, 2) \times (1, 2)$.

The modelling parameters used in the test are $c_x = c_y = 0{\cdot}4$, $R_{\Delta x} = R_{\Delta y} = 2$, $t = 1{\cdot}25$, $\alpha_x = \alpha_y = 0{\cdot}01$, $u = v = 0{\cdot}8$; that is, a snapshot of the travelling Gauss pulse is taken when it is centred at (1·5, 1·5) and then compared with the exact solution. Contour plots of the numerically approximated pulse in the subregion $x \in (1, 2)$, $y \in (1, 2)$ are drawn for each test carried out. The contour plots of the initial pulse in the subregion $x \in (0, 1)$, $y \in (0, 1)$ and the exact solution, which depict concentric circular contour lines for several selected contour values centred at $x = y = 1{\cdot}5$, are shown in Figures 12(a) and 12(b) respectively.

Test results are also presented in tabular form and include the average absolute error, the maximum absolute error, the minimum value of τ and the CPU time used. The minimum value

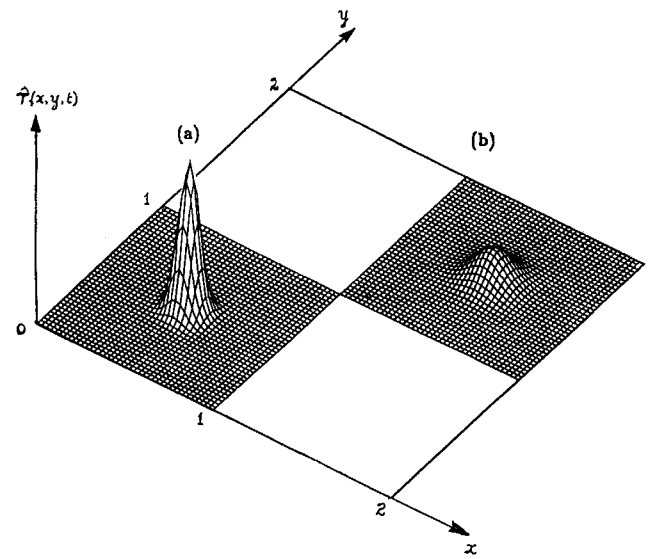

Figure 11. Three-dimensional perspective views of (a) the initial pulse and (b) the exact pulse after 1·25 s, for the numerical test

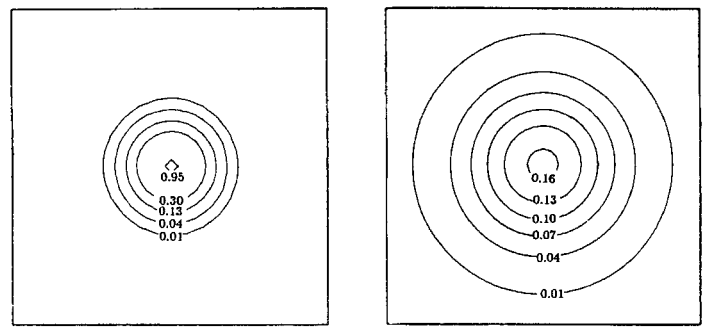

Figure 12. The contour plots of (a) the initial pulse in the subregion $\{x \in (0, 1)$ and $y \in (0, 1)\}$ and (b) the exact pulse after 1·25 s in the subregion $\{x \in (1, 2)$ and $y \in (1, 2)\}$

Table I. Numerical test results for explicit FDMs; $R_{\Delta x} = R_{\Delta y} = 2$, $c_x = c_y = 0{\cdot}4$, $t = 1{\cdot}25$

Method	Average |error|	Maximum |error|	Minimum τ	CPU time
FTCS	$3{\cdot}94 \times 10^{-3}$	$1{\cdot}12 \times 10^{-1}$	0	69 s
Upwind*	$2{\cdot}65 \times 10^{-3}$	$6{\cdot}63 \times 10^{-2}$	0	136 s*
Lax–Wendroff	$1{\cdot}74 \times 10^{-3}$	$2{\cdot}34 \times 10^{-2}$	0	96 s
Second-order (1, 9)	$3{\cdot}33 \times 10^{-4}$	$6{\cdot}03 \times 10^{-3}$	0	98 s

* The method is unstable for these parameters so $c_x = c_y = 0{\cdot}2$ with $R_{\Delta x} = R_{\Delta y} = 2$ were used instead. The smaller time step involved meant a larger CPU time than for the FTCS method.

Table II. Numerical test results for implicit FDMs; $R_{\Delta x} = R_{\Delta y} = 2$, $c_x = c_y = 0{\cdot}4$, $t = 1{\cdot}25$

Method	Average |error|	Maximum |error|	Minimum τ	CPU time
Single-sweep (2, 5)	5.72×10^{-4}	$1{\cdot}24 \times 10^{-2}$	$-1{\cdot}12 \times 10^{-5}$	63 s
Double-sweep (2, 5)	$6{\cdot}35 \times 10^{-4}$	1.30×10^{-2}	-4.56×10^{-9}	65 s
Single-sweep (2, 9)	$5{\cdot}69 \times 10^{-4}$	$1{\cdot}26 \times 10^{-2}$	$-8{\cdot}52 \times 10^{-6}$	96 s
Double-sweep (2, 9)	$6{\cdot}41 \times 10^{-4}$	$1{\cdot}32 \times 10^{-2}$	$-2{\cdot}63 \times 10^{-9}$	98 s
Crank–Nicolson (5, 5)	$3{\cdot}37 \times 10^{-4}$	$8{\cdot}70 \times 10^{-3}$	0	19087 s
Alternative (5, 5) (33)	$2{\cdot}56 \times 10^{-4}$	$6{\cdot}25 \times 10^{-3}$	0	25724 s
Alternative (5, 5) (37)	$2{\cdot}01 \times 10^{-4}$	$2{\cdot}68 \times 10^{-3}$	0	26646 s
Alternative (5, 5) (40)	$2{\cdot}01 \times 10^{-4}$	$2{\cdot}68 \times 10^{-3}$	0	25257 s
Third-order (9, 9)	$1{\cdot}43 \times 10^{-5}$	$4{\cdot}84 \times 10^{-4}$	0	30851 s

has been included to indicate whether negative values appear in a solution which should be always positive. This has particular application to the modelling of transfer of solutes, for example, as negative values of concentration have no physical meaning.

Explicit methods

Test results for the four explicit FDMs are listed in Table I and the corresponding contour plots are shown in Figure 13. All three (1, 5) methods suffer from the presence of inbuilt numerical

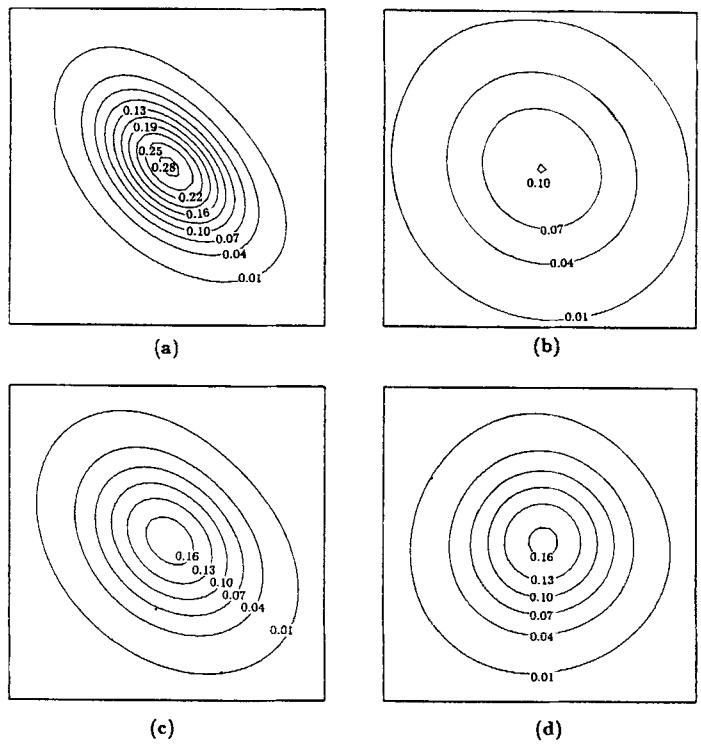

Figure 13. Contour plots of the numerical approximation at $t = 1{\cdot}25$ s for (a) the FTCS method, (b) the upwind method, (c) the improved (1, 5) method and (d) the explicit (1, 9) method

diffusion which is evident in the contour plots. The effect of the numerical anti-diffusion of the FTCS method is seen in the distribution of the contour lines in Figure 13(a), which show a higher pulse height than the exact solution shown in Figure 12(b). On the other hand, the numerical diffusion of the upwind method is evident in the lower pulse height in Figure 13(b). The contour plot for the Lax–Wendroff-type method in Figure 13(c) shows that the pulse has the correct height but its width has been compressed in the direction of propagation, indicative of the nature of the first-order error associated with the cross-derivative $\partial^2\tau/\partial x\partial y$.

These results are clearly explained by reference to the MEPDE of each method. Using transformed equations given in the Appendix, it is seen that the true solution of the model problem involves the initial Gauss peak being translated at speed $u\sqrt{2}$, $u = 0{\cdot}4$, along the line $y = x$ with diffusivity of $\alpha = 0{\cdot}01$ acting in the same direction (considered the X-axis in the following) and perpendicular to it (the Y-axis), namely

$$\frac{\partial \hat{t}}{\partial t} + u\sqrt{2}\frac{\partial \hat{t}}{\partial X} - \alpha\frac{\partial^2 \hat{t}}{\partial X^2} - \alpha\frac{\partial^2 \hat{t}}{\partial Y^2} = 0. \tag{62}$$

The total diffusivity acting in the directions is 2α, the same as in the x–y system.

By transforming its MEPDE, it is seen that use of the FTCS equation is equivalent to solving the PDE

$$\frac{\partial \tau}{\partial t} + u\sqrt{2}\frac{\partial \tau}{\partial X} - \frac{\alpha}{5}\frac{\partial^2 \tau}{\partial X^2} - \alpha\frac{\partial^2 \tau}{\partial Y^2} = 0. \tag{63}$$

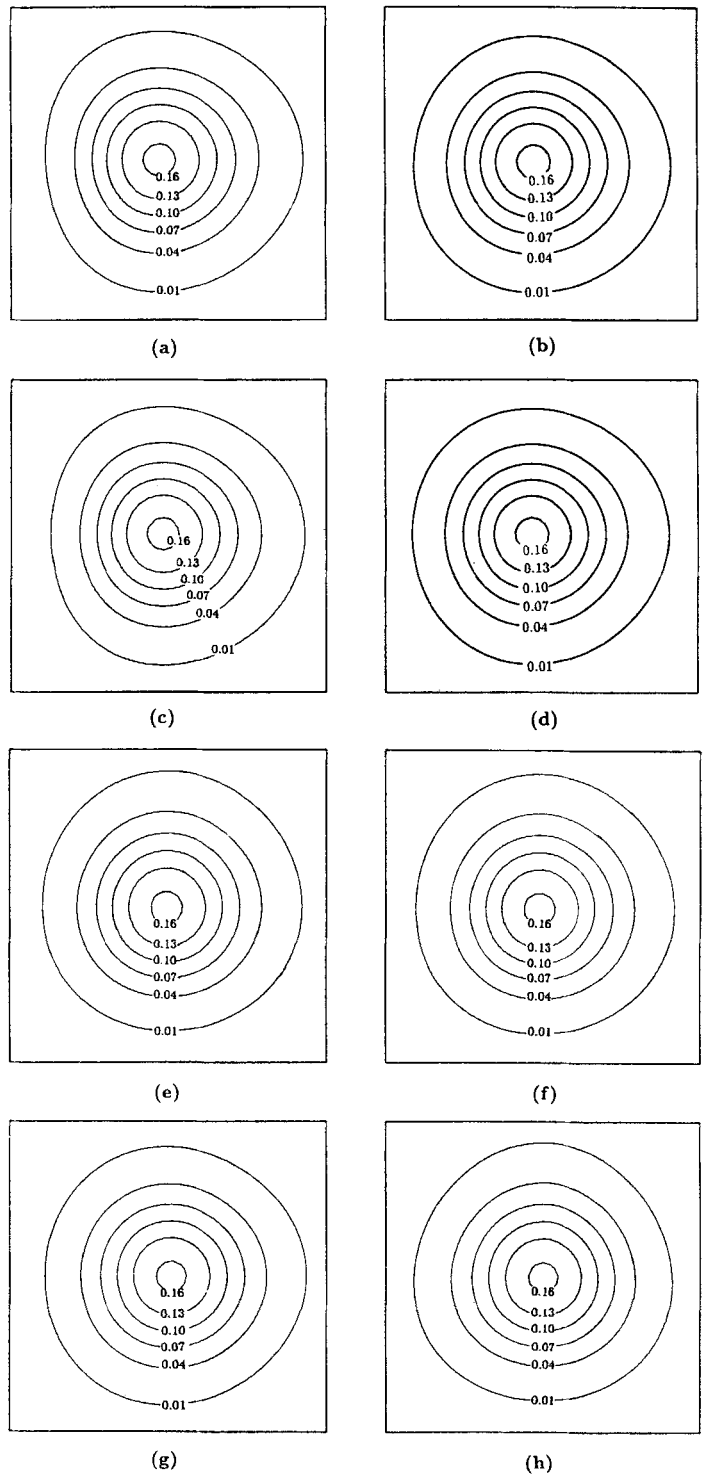

Figure 14

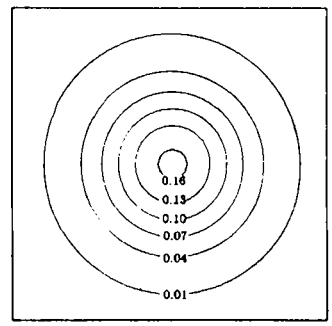

(i)

Figure 14. Contour plots of the numerical solutions at $t = 1{\cdot}25$ s for (a) the (2, 5) semi-implicit method, (b) the (2, 5) double-sweep method, (c) the (2, 9) semi-implicit method, (d) the (2, 9) double-sweep method, (e) the Crank–Nicolson-type method, (f) the alternative (5, 5) method, equation (33), (g) the alternative (5, 5) method, equation (37), (h) the alternative (5, 5) method, equation (40) and (i) the third-order (9, 9) method

The total diffusivity is $6\alpha/5$; this is smaller than in the true solution, which explains the higher peak in the numerical result. The reduction of the diffusion along the X-direction (the line $y = x$) is clear in the peaking of the results shown in Figure 13(a), with little change being evident in the diffusion along the Y-direction (the line $y = -x$). This asymmetry in diffusivity produces the elliptically shaped contour lines shown.

The upwind method is equivalent to solving the PDE

$$\frac{\partial \tau}{\partial t} + u\sqrt{2}\frac{\partial \tau}{\partial X} - \frac{6\alpha}{5}\frac{\partial^2 \tau}{\partial X^2} - 2\alpha\frac{\partial^2 \tau}{\partial Y^2} + \ldots = 0. \tag{64}$$

The total diffusivity is $16\alpha/5$, which is much larger than in the true solution; this explains the suppression of the peak in the numerical solution. In both the X- and Y-directions the diffusivity is larger than it should be, the larger value in the Y-direction causing a greater spread of the contour lines in that direction.

Use of the Lax–Wendroff-type method is equivalent to solving the PDE

$$\frac{\partial \tau}{\partial t} + u\sqrt{2}\frac{\partial \tau}{\partial X} - \frac{3\alpha}{5}\frac{\partial^2 \tau}{\partial X^2} - \frac{7\alpha}{5}\frac{\partial^2 \tau}{\partial Y^2} + \ldots = 0. \tag{65}$$

The total diffusivity in this equation is the same as in (62), which explains why the peaks in the numerical and true solutions have almost the same height. The smaller diffusivity in the X-direction compared with that in the Y-direction explains the crowding of the contour lines in the x-direction and their resultant elliptical shape. Because of the different diffusivities in the X- and Y-directions in (64), owing to the cross-derivative term in the MEPDE, it is clear that the coefficient $C_{1,1}$ must be made zero as well as the coefficients $C_{2,0}$ and $C_{0,2}$ if the diffusivities in the X- and Y-directions are to have the correct values of α. That is, the numerical method must be made second-order accurate.

The explicit second-order (1, 9) FDM, being completely free of first-order error terms, has average and maximum errors about one-tenth of the Lax–Wendroff-type method. The contour plot in Figure 13(d) shows a pulse of about the right height with the contour lines almost circular. The slight distortion in the pattern of these lines is due to the second-order error terms involving the third-order derivatives, which are connected with wave speed errors.

Implicit methods

Test results for the seven implicit FDMs are given in Table II and the corresponding contour plots in Figures 14. All the implicit methods except the (9, 9) FDM are second-order accurate and this is reflected in the average absolute errors in Table II. Since they are free of first-order error terms which introduce numerical diffusion, the Gauss pulse of each of these second-order methods has very nearly the correct peak height. However, the pulse distribution is distorted slightly owing to the wave speed error associated with the second-order error terms (see Figure 14). A noteworthy point is that the three alternative (5, 5) FDMs have the pulse distorted differently (about different axes of symmetry) owing to that fact that their different second-order error terms are related differently to the wave numbers in the x- and y-directions. It follows that the wave speed errors of these methods are different in the x- and y-directions. The same applies to the semi-implicit methods. It should also be noted that the use of the double-sweep procedure with the semi-implicit methods reduces the distortion of the circular contours in the numerical solution, as well as reducing the largest negative value by several orders of magnitude.

The third-order (9, 9) FDM has errors an order of magnitude less than those of the second-order FDMs. The resulting Gauss pulse is almost indistinguishable from the exact solution with the naked eye.

Within the accuracy of the computation (double precision on a VAK-11/780 minicomputer), for the test problem none of the explicit methods produced negative values in the numerical solution, nor did any of the fully implicit methods. However, both semi-implicit methods produced some small negative values, the worst being of the order of 10^{-5}. However, the double-sweep alternative reduced this to approximately 10^{-9} at the expense of slightly increased average and maximum errors.

In terms of CPU time taken, the semi-implicit second-order methods are more efficient than the fully implicit second-order methods owing to the fact that the former are computed explicitly using marching and the latter involve solving very large systems of linear algebraic equations. However, they have much smaller usable regions in the (R_Δ, c) plane. From Table I, using the block Thomas algorithm takes about 3000 times more CPU time than using marching.

8. CONCLUSIONS

The two-dimensional modified equation method has been successfully used with weighted discretizations to develop several new explicit, implicit and semi-implicit finite difference methods for solving the linear, constant coefficient, two-dimensional advection–diffusion equation. Use of the modified equivalent equation permits a proper determination of the order of accuracy of finite difference methods in both one- and multi-dimensional cases. In particular it gives an idea of the wave propagation characteristics of the methods.[11]

The finite difference methods developed in this paper vary in their order of accuracy and the size of their stability regions. Nonetheless, they are generally more accurate and possess larger stability regions than conventional explicit methods such as the FTCS and the upwind methods. The price to pay for such advantages is the increase in computational time due to the presence of more gridpoints and more complicated coefficients in the FDEs, in particular for the (5, 5) and (9, 9) FDMs. However, in the case of the (5, 5) FDM, time splitting the equation into its alternating direction implicit (ADI) form[23] permits the multiple use of the one-dimensional Thomas algorithm with a considerable saving in time over the use of the block Thomas form. This splitting is not possible with the (9, 9) FDM.

Development of more efficient third-order (6, 9) implicit methods, which use either marching or the same solution technique as the ADI method, will be reported in a future paper.

ACKNOWLEDGEMENTS

The authors thank K. Hayman and P. Steinle for their assistance with the computing work carried out, and the reviewers for their constructive criticism which improved the final version of this article. The second author was supported by a Singapore Government Scholarship during the period of this research.

APPENDIX: THE TRANSFORMED ADVECTION–DIFFUSION EQUATION

If the (x, y) co-ordinate system is rotated anti-clockwise by θ radians to form a new (X, Y) system, then the partial differential equation

$$\frac{\partial \tau}{\partial t} + u\frac{\partial \tau}{\partial x} + v\frac{\partial \tau}{\partial y} - \alpha_{xx}\frac{\partial^2 \tau}{\partial x^2} - \alpha_{xy}\frac{\partial^2 \tau}{\partial x \partial y} - \alpha_{yy}\frac{\partial^2 \tau}{\partial y^2} + \ldots = 0 \tag{66}$$

transforms to

$$\frac{\partial \tau}{\partial t} + U\frac{\partial \tau}{\partial X} + V\frac{\partial \tau}{\partial Y} - \alpha_{XX}\frac{\partial^2 \tau}{\partial X^2} - \alpha_{XY}\frac{\partial^2 \tau}{\partial X \partial Y} - \alpha_{YY}\frac{\partial^2 \tau}{\partial Y^2} + \ldots = 0, \tag{67a}$$

in which

$$\begin{aligned} U &= u\cos\theta + v\sin\theta, \\ V &= -u\sin\theta + v\cos\theta, \\ \alpha_{XX} &= \alpha_{xx}\cos^2\theta + \alpha_{xy}\sin\theta\cos\theta + \alpha_{yy}\sin^2\theta, \\ \alpha_{XY} &= 2\sin\theta\cos\theta(\alpha_{yy} - \alpha_{xx}) + \alpha_{xy}(\cos^2\theta - \sin^2\theta), \\ \alpha_{YY} &= \alpha_{xx}\sin^2\theta - \alpha_{xy}\sin\theta\cos\theta + \alpha_{yy}\cos^2\theta. \end{aligned} \tag{67b}$$

Note that

$$\begin{aligned} u^2 + v^2 &= U^2 + V^2, \\ \alpha_{xx} + \alpha_{yy} &= \alpha_{XX} + \alpha_{YY}. \end{aligned} \tag{67c}$$

In the model problem, $u = v$, $\alpha_{xx} = \alpha_{xy} = \alpha$ and $\theta = \pi/4$ radians, so the equation being solved is

$$\frac{\partial \hat{\tau}}{\partial t} + u\frac{\partial \hat{\tau}}{\partial x} + u\frac{\partial \hat{\tau}}{\partial y} - \alpha\frac{\partial^2 \hat{\tau}}{\partial x^2} - \alpha\frac{\partial^2 \hat{\tau}}{\partial y^2} = 0, \tag{68}$$

the transformed equation being

$$\frac{\partial \hat{\tau}}{\partial t} + u\sqrt{2}\frac{\partial \hat{\tau}}{\partial X} - \alpha\frac{\partial^2 \tau}{\partial X^2} - \alpha\frac{\partial^2 \hat{\tau}}{\partial Y^2} = 0. \tag{69}$$

Note that (68) translates the initial profile of $\hat{\tau}$ at speed $u\sqrt{2}$ in the X-direction and diffuses it in the X- and Y-directions by the same amount as in the x- and y-directions.

If the MEPDE of a FDM for solving (68) is

$$\frac{\partial \tau}{\partial t} + u\frac{\partial \tau}{\partial x} + u\frac{\partial \tau}{\partial y} - (\alpha - C)\frac{\partial^2 \tau}{\partial x^2} + D\frac{\partial^2 \tau}{\partial x \partial y} - (\alpha - C)\frac{\partial^2 \tau}{\partial y^2} + \ldots = 0, \tag{70}$$

then the transformed MEPDE is

$$\frac{\partial \tau}{\partial t} + u\sqrt{2}\frac{\partial \tau}{\partial X} - \alpha(1-E-F)\frac{\partial^2 \tau}{\partial X^2} - \alpha(1-E+F)\frac{\partial^2 \tau}{\partial Y^2} + \ldots = 0, \tag{71a}$$

where

$$E = C/\alpha, \qquad F = D/(2\alpha). \tag{71b}$$

REFERENCES

1. J. Isenberg and C. Gutfinger, 'Heat transfer to a draining film', *Int. J. Heat Transfer*, **16**, 505–512 (1972).
2. J. Y. Parlarge, 'Water transport in soils', *Ann. Rev. Fluid Mech.*, **2**, 77–102 (1980).
3. Q. N. Fattah and J. A. Hoopes, 'Dispersion in anisotropic, homogeneous, porous media', *J. Hydraul. Div., ASCE*, **111**, 810–827 (1985).
4. J. Bear and D. K. Todd, 'The transition zone between fresh and salt waters in coastal aquifers', *University of California, Water Resources Contribution*, No. 29 (1960).
5. P. C. Chatwin and C. M. Allen, 'Mathematical models of dispersion in rivers and estuaries', *Ann. Rev. Fluid Mech.*, **17**, 119–149 (1985).
6. F. M. Holly, Jr. and J. M. Usseglio-Polatera, 'Dispersion simulation in two-dimensional tidal flow', *J. Hydraul. Eng., ASCE*, **111**, 905–926 (1984).
7. J. R. Salmon, J. A. Liggett and R. H. Gallager, 'Dispersion analysis in homogeneous lakes', *Int. j. numer. methods eng.*, **15**, 1627–1642 (1980).
8. G. I. Taylor, 'Dispersion of solute matter in solvent flowing slowly through a tube', *Proc. Roy. Soc. Lond.*, **A219**, 186–203 (1953).
9. Z. Zlatev, R. Berkowicz and L. P. Prahm, 'Implementation of a variable stepsize variable formula method in the time-integration part of a code for treatment of long-range transport of air pollutants', *J. Comput. Phys.*, **55**, 278–301 (1984).
10. C. R. Gane and P. L. Stephenson, 'An explicit numerical method for solving transient combined heat conduction and convection problems', *Int. j. numer. methods eng.*, **14**, 1141–1163 (1979).
11. B. J. Noye, 'Finite difference techniques for partial differential equations', in B. J. Noye (ed.), *Computational Techniques for Differential Equations*, North-Holland Mathematics Studies, No. 83, 1984, pp. 95–354.
12. P. J. Roache, *Computational Fluid Dynamics*, Hermosa Publishers, Albuquerque, 1976.
13. B. J. Noye, 'Analysis of explicit finite difference methods used in computational fluid mechanics', in A. Miller (ed.), *Contributions of Mathematical Analysis to the Numerical Solutions of Partial Differential Equations; Proceedings of Centre for Mathematical Analysis, ANU, Vol. 7*, 1984, pp. 106–118.
14. B. J. Noye, 'Three-point two-level finite difference methods for the one-dimensional advection equation', in B. J. Noye and R. L. May (eds), *Computational Techniques and Applications: CTAC-85*, Elsevier Publishing Co., Amsterdam, 1986, pp. 159–192.
15. B. J. Noye and K. J. Hayman, 'An accurate five-point explicit finite difference method for solving the one-dimensional linear diffusion equation', in B.. J. Noye and R. L. May (eds), *Computational Techniques and Applications: CTAC-85*, Elsevier Publishing Co., Amsterdam, 1986, pp. 205–216.
16. B. J. Noye and K. J. Hayman, 'Accurate finite difference methods for solving the advection–diffusion equation', in B. J. Noye and R. L. May (eds), *Computational Techniques and Applications: CTAC-85*, Elsevier Publishing Co., Amsterdam, 1986, pp. 137–158.
17. B. J. Noye and H. H. Tan, 'A third order semi-implicit finite difference method for solving the one-dimensional convection–diffusion equation', *Int. j. numer. methods eng.*, **26**, 1615–1629 (1988).
18. B. J. Noye and H. H. Tan, 'Accurate five-point explicit finite difference methods for solving the one-dimensional transport equation', submitted to *Eng. Analysis* (1988).
19. A. C. Hindmarsh, P. M. Gresho and D. F. Griffiths, 'The stability of explicit Euler time-integration for certain finite difference approximations of the multi-dimensional advection–diffusion equation', *Int. j. numer. methods fluids*, **4**, 853–897 (1984).
20. L. H. Thomas, *Elliptic Problems in Linear Difference Equations over a Network*, Watkins Scientific Computing Laboratory, Columbia, New York, 1949.
21. D. G. Feingold and R. S. Varga, 'Block diagonally dominant matrices and generalizations of the Gershgorin Theorem', *Pacific J. Math.*, **12**, 1241–1250 (1962).
22. P. D. Lax and B. Wendroff, 'Difference schemes with high order of accuracy for solving hyperbolic equations', *Comm. Pure Appl. Math.*, **17**, 381–398 (1964).
23. J. Douglas, Jr., 'On the numerical integration of $\partial^2 u/\partial x^2 + \partial^2 u/\partial y^2 = \partial u/\partial t$ by implicit methods', *J. SIAM*, **3**, 42–65 (1955).